1 **Intermediate water masses, a major supplier of oxygen for the eastern tropical Pacific ocean**

2 Olaf Duteil (oduteil@geomar.de)(1), Ivy Frenger(1), Julia Getzlaff(1)

3 (1) GEOMAR, Kiel, Germany

5 **Abstract**

6 It is well known that Intermediate Water Masses (IWM) are sinking in high latitudes and ventilate

7 the lower thermocline (500 – 1500 m depth). We here highlight how the IWM oxygen content and

8 the IWM pathway along the Equatorial Intermediate Current System (EICS) towards the eastern

9 tropical Pacific ocean are essential for the supply of oxygen to the lower thermocline and the

10 Oxygen Minimum Zones (OMZs). To this end, we assess here a heterogeneous subset of ocean

11 models characterized by a horizontal resolution ranging from 0.1° to 2.8°. Subtropical oxygen

12 levels in the lower thermocline, i.e., IWM are statistically correlated with tropical oxygen levels and

13 OMZs. Sensitivity simulations suggest that the oxygen biases of the subtropical IWM oxygen levels

14 contribute to oxygen biases of the tropical thermocline : an increase of the IWM oxygen by 60

15 mmol.m^{-3} results in a 10 mmol.m^{-3} increase in the tropical ocean in a timescale of 50 years. In the

16 equatorial regions, the IWM recirculates into the Equatorial Intermediate Current System (EICS).

17 By comparing tracer and particle release simulations, we show that a developed EICS increases

18 eastern tropical ventilation by 30 %. Typical climate models lack in representing crucial aspects of

19 this supply: biases in IWM properties are prominent across climate models and the EICS is

20 basically absent in models with typical resolutions of ~1°. We emphasize that these biases need to

21 be reduced in global climate models to allow reliable projections of OMZs in a changing climate.

23 **1. Introduction**

24 Oxygen levels in the ocean are characterized by high values in the high latitudes and the subtropical

25 gyres, while concentrations decrease to close to zero in the tropical oceans in the Oxygen Minimum

26 Zones (OMZs). While OMZs are natural features, climate change is potentially responsible for their

27 expansion (Breitburg et al., 2018), leading to a reshaping of the ecosystems and a potential loss of

28 biodiversity. In order to perform robust projections there is a need to better understand the processes

29 at play that are responsible for the supply of oxygen to the OMZ. We focus here on the Pacific

30 ocean, where the largest OMZs are located (Karstensen et al., 2008; Paulmier and Ruiz-Pino. 2009)

32 Oxygen rich waters are supplied into the ocean by subduction processes (Karstensen et al., 2008).

33 Oxygen solubility increases with lower temperatures, thus waters formed in the Southern Ocean

34 and in the North Pacific are characterized by particularly high oxygen values. In particular, the

36   Antarctic Intermediate Water (AAIW) (Molinelli, 1981) ventilates large areas of the lower

37   thermocline of the Pacific Ocean (Sloyan and Rintoul., 2001) and is characterized by oxygen values

38   larger than 300 mmol.m^{-3} at subduction time (Russel and Dickson, 2003). The oxygenated core of

39   the AAIW in the tropical Pacific is located at about 500-1200 m depth at 40°S (Russell and

40   Dickson, 2003) and with this at a depth directly below the depth of the OMZs in the eastern Pacific;

41   the Pacific AAIW mixes down to 2000 m depth with the Pacific Deep Water (PDW) as determined

42   by the OMP (Optimum Multiparameter) analysis (Pardo et al., 2012; Carrasco et al., 2017). The

43   oxygen rich (> 200 mmol.m^{-3} at 40°S) AAIW spreads from its formation side in the Southern Ocean

44   to the subtropical regions ; conversely the oxygen poor PDW (below 150 mmol.m^{-3}), extends till

45   3000m depth and recirculates poleward (Koshlyakov and Tarakanov, 2003). The northern part of

46   the Pacific basin is characterized by the North Pacific Intermediate Water (NPIW) (Talley, 1993)

47   confined to the northern Pacific conversely to the AAIW, which spreads far northward as it

48   signature reaches 15°N (Qu and Lindstrom., 2004). AAIW, NPIW and the upper part of the PDW

49   are oxygenated water masses occupying the lower thermocline between 500 and 1500 m depth. We

50   will refer to these waters as Intermediate Water Masses (IWM) in the following.

51

52   In the subtropics, the IWM (more particularly the AAIW) circulates into the intermediate flow of

53   the South Equatorial Current and the New Guinea Coastal Undercurrent (Qu and Lindstrom, 2004)

54   where it retroflects in the zonal equatorial flows of the Southern Intermediate Countercurrent

55   (SICC) and Northern Equatorial Intermediate Current (NEIC) within about ±2° off the equator

56   (Zenk et al., 2005; Kawabe et al., 2010) (Fig 1). These currents are part of the Equatorial

57   Intermediate Current System (EICS) constituted by a complex system of narrow jets extending

58   below 500 m in the lower thermocline (Firing, 1987; Ascani et al., 2010; Marin et al. 2010; Cravatte

59   et al., 2012, 2017; Menesguen et al., 2019). While the existence of this complex jet system has been

60   shown to exist in particular using argo floats displacements (Cravatte et al., 2017) the spatial

61   structure and variability of the jets are still largely unknown. In addition, there is little knowledge

62   about their role in transporting properties such as oxygen.

63

64   The simulation of the supply of oxygen to the eastern tropical Pacific is a difficult task as it depends

65   on the realistic simulation of the IWM properties (in particular the oxygen content) and the IWM

66   pathway (through the EICS).   It is known that current climate models, in particular CMIP5

67   (Coupled Model Intercomparison Project phase 5) models, have deficiencies in correctly

68   representing the IWM, and in particular the AAIW. They generally display too shallow and thin

69   IWM, with a limited equatorward extension compared to observations (Sloyan and Kamenkovich,

70 2007; Sallee et al., 2013; Meijers, 2014; Cabre et l., 2015; Zhu et al., 2018 for the south Atlantic

71 ocean). Discrepancies in the simulated properties of IWM compared to observations are due to a

72 combination of many errors in the climate models, including simulation of wind and buoyancy

73 forcing, inadequate representation of subgrid-scale mixing processes in the Southern Ocean, and

74 midlatitude diapycnal mixing parameterizations (Sloyan and Kamakovich, 2007; Zhu et al., 2018).

75 In addition, the representation of the EICS is lacking in coarse resolution models (Dietze and

76 Loeptien, 2013; Getzlaff and Dietze, 2013). Higher resolution (0.25°, 1/12°) configurations partly

77 resolve the EICS but with a smaller amplitude than observed (Eden and Dengler, 2008; Ascani et

78 al., 2015). The mechanisms forcing the EICS are complex and still under debate (see the review by

79 Menesguen et al., 2019).

80

81 In this study we focus on the impact of IWM (and of the deficiencies in the representation of their

82 properties and transport) on the oxygen content in the eastern tropical Pacific in a set of model

83 simulations. Section 2 gives an overview of all models that we used as well as of the sensitivity

84 simulations. Next, we assess to which extent the IWM modulate (or drive) the oxygen levels in the

85 eastern tropical (20°S - 20°N) Pacific ocean in this set of models. The role of the IWM depends i)

86 on the oxygen content of the IWM in the lower thermocline of the subtropical regions (section 3)

87 and ii) on the zonal recirculation of the oxygen by the EICS toward the eastern part of the basin

88 (section 4). We conclude in section 5.

89

90 **2. Analyzed models and experiments**

91 2.1 Mean state

92 We analyze the mean state of the oxygen fields, OMZ, EICS of the following model experiments

93 (see Table 1), which previously have been used in recent studies focusing on the understanding of

94 the tropical oxygen levels mean state or variability:

95 - a NEMO (Nucleus for European Modelling of the Ocean) configuration with a resolution of 2°,

96 refined meridionally to 0.5° in the equatorial region (NEMO2). The circulation model is coupled to

97 a simple NPZD (Nutrient Phytoplankton Zooplankton Detritus) biogeochemical model that

98 comprises 6 compartments (e.g used in Duteil et al., 2018; Duteil, 2019). The simulation has been

99 forced by climatological forcings based on the Coordinated Reference Experiments (CORE) v2

100 reanalysis (1948-2007) (Large and Yeager, 2009) and integrated for 1000 years.

101 - the UVIC (University of Victoria) model (e.g used in Getzlaff et al., 2016; Oschlies et al., 2017),

102 an earth System Model (ESM) that has a horizontal resolution of 1.8° latitude x 3.6° longitude. The

103 experiment has been integrated for 10000 years. The biogeochemical model is a NPZD-type model

104 of intermediate complexity that describes the full carbon cycle (see Keller Keller 2012 for a detailed

105 description). This model is forced by monthly climatological NCAR/NCEP wind stress fields.

106 - the GFDL (Geophysical Fluid Dynamics Laboratory) CM2-0 suite (Delworth et al., 2012; Griffies

107 et al., 2015, Dufour et al, 2015): the suite is based on the GFDL global climate model and includes

108 a fully coupled atmosphere with a resolution of approximately 50 km. It consists of three

109 configurations that differ in their ocean horizontal resolutions: GFDL1 with a nominal 1°

110 resolution, GFDL025 with a nominal 0.25° and GFDL01 with a nominal 0.1° resolution (e.g used in

111 Frenger et al., 2018 and Busecke et al., 2019 for studies on ocean oxygen). The climate models are

112 forced with preindustrial atmospheric pCO2 concentrations. At simulation year 48, the simplified

113 ocean biogeochemistry model miniBLING is coupled to the models, with three prognostic tracers,

114 phosphate, dissolved inorganic carbon and oxygen (Galbraith et al., 2015). Due to the high

115 resolution of GFDL01, the integration time is limited. We here analyze simulation years 186 to 190.

116 The heterogeneity of the configurations that we analyze permits to determine whether the simulated

117 oxygen distributions of the models display systematic biases or are strongly configuration

118 dependent (e.g dependent on resolution).

119

120 2.2 Sensitivity simulations

121 In order to disentangle the different processes at play we perform two different sets of sensitivity

122 simulations with one of the models, NEMO. NEMO allows to test effects of increasing the ocean

123 resolution and to integrate the model over a relatively long time span. All sensitivity experiments

124 are integrated for more than 50 years (1948 to 2007) using the CORE (Coordinated Ocean-Ice

125 Reference Experiments) v2 interannual (Large and Yeager, 2009) forcings. This time scale permits

126 the recirculation from the interior subtropical regions to the tropical area (as suggested in the model

127 study by SenGupta and England, 2007).

128

129 2.2.1 Oxygen restoring to observations in the subtropical regions

130 In the first set of experiments the focus is on the role of the lower thermocline oxygen content for

131 the ventilation of the eastern equatorial Pacific. We use NEMO2, the oceanic component of the

132 IPSL-CM5A (Mignot et al., 2013), that is part of CMIP5. NEMO2 shows mid-latitudes oxygen

133 biases consistent with CMIP5 models. We compare three experiments :

134 - NEMO2-REF: the experiment is integrated from 1948 to 2007 starting from the spinup state

135 described in 2.1.

136   - NEMO2-30DEG: the oxygen boundaries are restored to observed oxygen concentrations (WOA)

137   at the boundaries 30°N and 30°S : the mid-latitude supply of oxygen by the IWM is therefore

138   correctly represented.

139   - NEMO2-30DEG1500M: same as NEMOO2-30DG ; in addition oxygen is also restored at the

140   depth interface of 1500m, mimicking a correct oxygen state of the deeper water masses (lower part

141   of the AAIW, upper part of the PDW)

142

143   We focus with the above three experiments on the transport of IWM oxygen levels to the tropical

144   ocean and the OMZs. The respiration rate (oxygen consumption) is identical in NEMO2-REF,

145   NEMO2-30DEG and NEMO2-30DEG1500M in order to avoid compensating effects between

146   supply and respiration that depends on biogeochemical parameterizations (e.g Duteil et al., 2012).

147   We aim to avoid such compensating effects to ease interpretation and be able to focus on the role of

148   physical transport.

149

150   2.2.2 Conservative Tracer Release in oxygenated waters

151   In a second set of experiments, we performed tracer release experiments in a coarse 0.5°

152   (NEMO05) and high resolution 0.1° (NEMO01) configurations of NEMO (Table 1) to examine the

153   transport of oxygenated IWM from the subtropical regions into the oxygen deficient tropics.

154   NEMO01 is a configuration based on NEMO05 and where a 0.1° two-ways nest has been

155   embedded in the whole Pacific Ocean, from 49°S to 31°N (Czeschel et al, 2011). In these

156   experiments, we initialized the regions with climatological (WOA) oxygen levels greater than 150

157   mmol.m^{-3} with a value of 1 (and 0 when oxygen is lower than 150 mmol.m^{-3}). In the model

158   simulations, the tracer is subject to the same physical processes as other physical and

159   biogeochemical tracers, i.e. advection and diffusion but it does not have any sources and sinks. The

160   experiments have been integrated for 60 years (1948 – 2007) using realistic atmosphere forcing

161   (COREv2). NEMO05 and NEMO01 display a similar upper ocean circulation (Fig 5) but NEMO05

162   does not simulate a developed EICS contrary to NEMO01.

163

164   In order to complement the tracer experiment we performed Lagrangian particle releases.

165   Lagrangian particles allow to trace the pathways of water parcels due to the resolved currents, and

166   to track the origin and fate of water parcels. They are not affected by subgrid scale mixing

167   processes. The particles are advected offline with 5 daily means of the NEMO05 and NEMO01

168   currents. The NEMO01 circulation fields have been interpolated on the NEMO05 grid in order to

169   allow a comparison of the large scale advective patterns between NEMO01 and NEMO05. We used

170 the ARIANE tool (Blanke and Raynaud, 1997). A first particle release has been performed in the

171 eastern tropical OMZ at 100°W in the tropical region between 5°S - 5°N, a second release has been

172 performed in the western part of the basin at 160°E The particles have been released in the lower

173 thermocline at 1000 m and integrated backward in time from 2007 to 1948 in order to determine

174 their pathways and their location of origin. We released 120 particles every 5 days during the last

175 year of the experiment, for a total of 8760 particles.

176

3. Intermediate water properties and oxygen content

177

3.1. IWM Oxygen levels in models

178

179 The IWM subducted in mid/high latitudes are highly oxygenated waters. As part of the deficient

180 representation of IWM, the subducted "oxygen tongue" (oxygen values up to 240 mmol.m^{-3}) is not

181 reproduced in most of the models part of CMIP5 (Fig 8 from Cabre et al., 2015, Fig 4 from Takano

182 et al., 2018) and in the models analyzed here (Fig 2a), with biases of about 20-60 mmol.m^{-3}

183 (NEMO2, GFDL1, GFDL025, GFDL01). UVIC, a coarse resolution model, shows oxygenated

184 waters in the lower thermocline at mid latitudes (30°S-50°S); the oxygenation however arises due to

185 a too large vertical diffusion from the mixed layer rather than by an accurate representation of the

186 water masses. GFDL01, even though still biased low, presents larger oxygen values than the coarser

187 resolution models GFDL1, GFDL025 and NEMO2. A possible explanation is a better

188 representation of the water masses and in particular the AAIW in eddy-resolving models (Lackhar

189 et al., 2009). The IWM oxygen maximum is apparent at 30°S throughout the lower thermocline in

190 observations (Fig 2b), consistent with the circulation of IWM with the gyre from the mid/high

191 latitude formation regions towards the northwest in subtropical latitudes, and followed by a

192 deflection of the waters in the tropics towards the eastern basin.

193

194 Consistent with the low oxygen bias of models at subtropical latitudes (Fig 2b), models also feature

195 a bias in the tropical ocean (20°S-20°N) by 20 – 50 mmol.m^{-3} (Fig 2a, Fig 2c) at intermediate depths

196 in the eastern part of the basin (similarly to CMIP5 models, as shown by Cabre et al., 2015). The

197 basin zonal average of the mean oxygen level in the lower thermocline (layer 500 - 1500) m at 30°S

198 and in the eastern part of the basin (average 20°S – 20°N, 160°W-coast; 500-1500 m) are positively

199 correlated (Pearson correlation coefficient R=0.73) (Fig 2d), suggesting a large role of the IWM in

200 controlling the oxygen levels in the tropical oceans.

201

202 The models presenting the poorest oxygenated water at 30°S display the largest volume of OMZs

203 (GFDL025 and GFDL1), though the negative correlation (Pearson correlation coefficient R=-0.52)

204   is less pronounced between the volume of the OMZs and the mean oxygen levels in the layer 500 -

205   1500 m at 30°S (Fig 2e). Reasons of this weaker correlation are due to the OMZs being a result of

206   several processes next to oxygen supply by IWM, e.g, vertical mixing with other water masses

207   (Duteil et al., 2011), isopycnal mixing in the upper thermocline (Gnanadesikan et al., 2013; Bahl et

208   al., 2019), supply by the upper thermocline circulation (Shigemitsu et al., 2017; Busecke et al.,

209   2019). A correlation, even weak, suggests a major role of the IWM in regulating the OMZ volume

210

211   In order to better understand the role of IWM entering the subtropical domain from higher latitudes

212   for the oxygen levels in the eastern tropical Pacific Ocean, we perform sensitivity experiments (see

213   2.2.1) in the following.

214

215   3.2 Sensitivity of tropical IWM oxygen to subtropical and deep oxygen levels

216   3.2.1 Oxygen levels in the lower thermocline

217   The difference of the experiments NEMO2-30DEG – NEMO2-REF (average 1997-2007) allows to

218   quantify the effect of model biases of IWM at mid latitudes (30°N/30°S). As we restore oxygen to

219   observed levels at 30°S/°N (see 2.2.1), the difference shows a large anomaly in oxygen levels at

220   30°S (more than 50 mmol.m^{-3}) at lower thermocline level (500 – 1500 m) corresponding to the

221   missing deep oxygen maximum (Fig 3). The northern negative anomaly results from a deficient

222   representation of the north Pacific OMZ, i.e., modeled oxygen is too high for NPIW. The northern

223   low and southern high anomalies spread towards the tropics at intermediate depth. A fraction of the

224   positive oxygen anomaly recirculates at upper thermocline level due to a combination of upwelling

225   and zonal advection by the tropical current system (for instance the EUC at thermocline level is a

226   major supplier of oxygen as shown in observations by Stramma et al., 2010 and in ocean models by

227   Duteil et al., 2014, Busecke et al., 2019).

228

229   The difference NEMO2-30DEG1500M – NEMO2-30DEG (Fig 3f-h) shows a deep positive

230   anomaly in oxygen, as oxygen levels are lower than in observations by 30-40 mmol.m^{-3} in the

231   eastern tropical regions. This anomaly is partially transported into the lower thermocline (500 -

232   1500 m). It shows that a proper representation of the deep oxygen level (> 1500 m) is important for

233   a realistic representation of the lower thermocline and OMZs. Causes of the oxygen bias of the

234   deeper water masses are beyond the scope of this study but may be associated with regional

235   (tropical) issues, such as an improper parameterization of respiration (e.g a too deep

236   remineralisation) (Kriest et al., 2010), or a misrepresentation of deeper water masses.

237

3.2.2 Oxygen budget and processes

238
239 To assess the processes that drive the oxygen content of the (sub)tropical lower thermocline, we
240 analyzed the oxygen budget in NEMO2-REF and NEMO2-30DEG. The budget is calculated as an
241 average between 500 and 1500m and shown in Fig.4. In NEMO2-REF, the physical oxygen supply
242 is balanced by the respiration. The oxygen supply in the model is divided into advection, i.e.,
243 oxygen transport associated with volume transport, and isopycnal diffusion, i.e., subgrid scale
244 mixing processes that homogenize oxygen gradients. Diapycnal diffusion is comparatively small
245 and can be neglected. The lower branches of the subtropical gyres transport the oxygen from the
246 eastern to the western part of the basin (Fig 4a,b). Downwellings from the oxygen-rich upper layer
247 supply the interior of the subtropical gyres (Fig 4c). At the equator, the EICS transport westward
248 oxygen-poor water originating in the eastern side of the basin (Fig 4a). Concomitantly, the
249 meridional advection term transports oxygen originating from the subtropics in the tropical regions
250 (Fig 4b), which is upwelled (Fig 4c). Isopycnal diffusion transfers oxygen from the oxygen-rich
251 gyres to the poor oxygenated regions (Fig 4d).

252

253 The anomalies generated at 30°S and 30°N by the restoring experiment generate a disbalance
254 between respiration (which remains identical in NEMO2-REF and NEMO2-30DEG) and supply.
255 This disbalance is most apparent in the tropics by an increase (south) or decrease (north) of
256 isopycnal diffusion (Fig 4g, Fig 3h). Changes in the advective terms can be found along the
257 equator: as the vertical gradient of oxygen decrease (the intermediate ocean being more
258 oxygenated), the vertical supply from the upper ocean decreases in the south (increases in the north)
259 subtropical gyre and decreases at the equator (Fig 4g). The meridional oxygen gradient between the
260 southern subtropical gyre and the equator strengthens, and so the meridional transport from the
261 subtropics to the equator, partly by the western boundary currents (Fig 4f). The changes in zonal
262 transport are comparatively small (Fig 4e). The total advective term does not show significant
263 change however (Fig 4g).

264

265 In the experiment NEMO2-30DEG1500, in complement to the isopycnal propagation of the
266 subtropical anomaly, the deep (> 1500 m) oxygen anomaly is upwelled in the eastern equatorial
267 (500 – 1500 m) part of the basin (see Fig 4i) showing a large increase in advective terms, mostly
268 due to an increase in vertical advection), consistent with the analysis by Duteil (2019) who showed
269 that vertical advection is the dominant process to supply oxygen from the lower to the upper
270 thermocline in the equatorial eastern Pacific Ocean in a similar NEMO2 configuration.

271

272   This simple set of experiment shows that in climate models oxygen in the lower thermocline (500 –

273   1500 m) ocean are partially controlled by properties of IWM that enter the tropics from higher

274   latitudes. This presumably applies to other (biogeochemical) tracers. IWM oxygen propagates

275   equatorward mostly by small scale isopycnal processes and the western boundary currents. Further,

276   upwelling in the tropics from deeper ocean layers (Pacific Deep Water, partially mixed with the

277   lower IWM) play an important role . Our budget analysis highlighted the importance of advective

278   processes in the equatorial region in the lower thermocline which we will examine more closely in

279   the following.

280

281   **4. Equatorial intermediate current system and oxygen transport**

282   4.1 Structure of the currents in the upper 2000 m in observations and models

283   The current structure of the models analyzed in this study (see section 2.1, Table 1) is shown in Fig.

284   5. In the upper layer, the broad westward drifting South and North Equatorial Currents (SEC, NEC)

285   characterize the equatorial side of subtropical gyres. In the thermocline, the eastward flowing

286   equatorial undercurrent (EUC), flanked by the westward flowing south and north counter currents

287   are present in all models. This upper current structure is well reproduced (i.e the spatial structure

288   and intensity are consistent with observations) across the different models (see 2.1 "Model

289   analyzed") compared to observations. Previous studies already discussed the upper thermocline

290   current structure in the GFDL models suite (Busecke et al., 2019), NEMO (e.g Izumo, 2005,

291   Lübbecke et al., 2008), UVIC (Loeptien and Dietze, 2013); the upper thermocline will not be

292   further discussed in this study.

293

294   At intermediate depth, in the observations, a relatively strong (about 0.1 ms^{-1}) westward flowing

295   Equatorial Intermediate Current (EIC) is present below the EUC at about 400-600 m depth (Marin

296   et al., 2010). A complex structure of narrow and vertically alternating jets every 200 m, so-called

297   Equatorial Deep Jets (EDJ), extends below the EIC till 2000 m (Firing, 1987; Cravatte et al., 2012).

298   Laterally to the EIC, in the upper thermocline, the Low Latitude Subsurface Countercurrents

299   (LLSC) are observed. They include the North and South Subsurface Counter Currents (NSCC and

300   SSCC), located around 5°N/5°S, and a series of jets between 5°N/S and 15°N/S (in particular the

301   Tschuya jets in the southern hemisphere, described by Rowe et al., 2000). Below the LLSCs, the

302   Low Latitude Intermediate Currents (LLICs) include the a series of westward and eastward zonal

303   jets (500–1500-m depth range) alternating meridionally from 3°S to 3°N; the North and South

304   Intermediate Countercurrents (NICC and SICC) flow eastward at 1.5°–2° on both flanks of the

305   lower EIC. The North and South Equatorial Intermediate Currents (NEIC and SEIC) flow westward

306 at about 3° (Firing, 1987). A detailed schematic view of the tropical intermediate circulation is

307 shown in a recent review by Menesguen et al. (2019) and in Fig 1.

308

309 In coarse resolution models, the intermediate current system is not developed and sluggish (even

310 missing in UVIC and GFDL1). NEMO2 and NEMO05 display a "primitive" EICS as the LLSCs

311 are not represented. High resolution models (GFDL025, GFDL01, NEMO01) display a more

312 realistic picture, even if the mean velocity is still weaker than in observations (smaller than 5 cm.s^{-}

313 ^{1}), where it reaches more than 10 cm^{-1} at 1000 m (Ascani et al., 2010; Cravatte et al., 2017). An

314 interesting feature is that the jets are broader and faster in NEMO01 than in GFDL01. Possible

315 causes include   a different wind forcing, mixing strength or topographic features as all these

316 processes play a role in forcing the intermediate jets (see the review by Menesguen et al., 2019).

317 The intermediate currents are less consistent vertically in NEMO01 than in GFDL01, due to their

318 large temporal variability in NEMO01. A strong seasonal and interannual variability of the EICS

319 has been observed that display varying amplitudes and somewhat positions of the main currents/jets

320 (Firing, 1998; Gouriou et al., 2006: Cravatte et al., 2017). A clear observational picture of the EICS

321 variability is however not yet available. Outside the tropics (in particular south of 15°S), the interior

322 velocity pattern is similar in coarse and high resolution models, suggesting a similar equatorward

323 current transport at intermediate depth in the subtropics, in for instance NEMO05 and NEMO01.

324

325 4.2 Transport by the EICS

326 4.2.1 Tracer spreading towards the eastern tropical Pacific

327 We released a conservative tracer in the subtropical domain in well oxygenated waters (see 2.2.2) in

328 a coarse (NEMO05) and a high resolution configuration (NEMO01). The tracer does not have

329 sources or sinks and is advected and mixed as any other model tracer and allows to assess the

330 spreading of tracer (such as oxygen) from oxygenated waters into the oxygen deficient eastern

331 tropical Pacific.

332

333 The ventilation by the oxygen rich waters, and in particular the IWM, is illustrated by the tropical

334 tracer concentration after 50 years (Fig 6a-c) of integration (mean 2002-2007). Concentrations

335 decrease from the release location to the northern part of the basin, where the lowest values (below

336 0.1) are located in NEMO05 and NEMO01. The 0.1 isoline is however located close to the equator

337 in NEMO05 while it is found around 7°N in NEMO01. This feature is associated with a pronounced

338 tongue of high tracer concentration (> 0.2) between 5°N and 5°S in NEMO1. Such a tongue is

339 absent in NEMO05. The enhanced tracer concentration in the equatorial region suggests a stronger
340 equatorial ventilation in NEMO01.

341

342 The preferential pathways of transport are highlighted by the determination of the transit time it
343 takes for the tracer to spread from the oxygen rich regions to the tropical regions. We define a
344 threshold called t10% when the tracer reaches a concentration of 0.1 (Fig 6d-f) (similar to the
345 approach of SenGupta and England, 2007). t10% highlights a faster ventilation of the equatorial
346 regions in NEMO01 compared to NEMO05, as t10% displays maximum value of 10 (western part)
347 to 30 years (eastern part) between 5°N/5°S in NEMO01 compared to 30 years to more than 50 years
348 in NEMO05. The southern "shadow zone" is well individualized in NEMO01 compared to
349 NEMO05 as the oxygen levels are high in the equator in NEMO01, suggesting a strong transport by
350 the EICS. While t10% increases linearly at intermediate depth at 100°W in NEMO05 from 20°S to
351 the equator, suggesting a slow isopycnal propagation (consistent with the experiments performed
352 using NEMO2 in part 3.2), the tracer accumulation is faster in the equatorial regions than in the
353 mid-latitudes in NEMO01, suggesting a large role of advective transport, faster than a transport by
354 diffusive processes.

355

356 4.2.2 Equatorial lower thermocline water mass origin
357 Lagrangian Particles (see 2.2.3) allow us to understand the origin of the waters in the lower
358 thermocline. They also allow to disentangle the transport of the resolved currents of the EICS
359 (advection) from subgrid scale mixing processes, i.e. to assess the processes responsible for the
360 equatorial ventilation. Two releases have been performed in the eastern and western part of the
361 basin in order to assess the equatorial circulation in NEMO05 and NEMO01.

362

363 The particles of the first release in the eastern tropical Pacific (100°W, at 1000 m depth where the
364 EICS are located) origin from the intermediate eastern tropical pacific (IETP) ocean (160°W – coast
365 / 10°N-10°S / 200 – 2000 m) close to the region of release, in 60 % of the cases in NEMO05 and
366 50 % of the cases in NEMO01, at a time scale of 50 years (Fig 7a-c and 8a). In NEMO05, after 50
367 years, the particles originating outside the IETP come either from the upper (0 – 200 m) ocean (5
368 %), deep (> 2000 m) ocean (1%), higher (> 10°) latitudes (23 %), western (west of 160°W) part of
369 the basin (21 %) (Fig 8c). The largest difference between NEMO05 and NEMO01 is the much
370 larger amount of particles originating from the deep ocean in NEMO01 (8 % in NEMO01),
371 suggesting the presence of vertical recirculation cells at intermediate depths. The advection
372 processes are also considerably faster in NEMO01, in particular the zonal advective ones. The

373 relative difference between NEMO05 and NEMO1 is particularly strong 15 years after the release

374 (approximately corresponding to the t10% at 1000 m at the equator in NEMO01), as already 10 %

375 of the particles originate outside the IETP, in regions where the oxygen levels are high, in NEMO01

376 while this fraction is close to 0 in NEMO05.

377

378 The particles of the second release (160°E, 1000 m depth) are originally located in the intermediate

379 western tropical pacific Ocean (IWTP) (160°W – coast / 10°N-10°S / 200 – 2000 m) (Fig 7e-f).

380 After 50 years, all the particles originate outside of this box in NEMO01 (Fig 8b) (50 % originate in

381 the eastern basin, 23 % in the deep ocean, 24 % outside the equatorial band, 3 % in the upper 200

382 m) (Fig 8d) while only 70 % of the particles originate outside the IWTP in NEMO05 (39 % in the

383 eastern basin, 27 % outside the equatorial band, 2 % in the deep ocean and 2 % in the upper ocean).

384

385 The Lagrangian particle results point to a generally stronger ventilation at intermediate depth in

386 NEMO01 due to the EICS, which reinforce the connection between western / eastern part of the

387 basin and thermocline / deep ocean

388

389 4.3 Equatorial oxygen levels in models

390 Our analyses above permit to better understand the distribution of the oxygen levels at the equator

391 in a suite of models characterized by an increasing resolution, such as the GFDL model suite. The

392 striking difference between GFDL01 and GFDL025 / GFDL1 are the high oxygen levels in the

393 eastern part of the ocean below 1000 m in GFDL01 compared to GFDL025/GFDL1 (Fig 2). The

394 oxygen levels are also more homogeneous zonally in GFDL01, with a weaker east/west gradient,

395 consistent with the tracer experiment that we performed in 4.2. The oxygen distribution fits with the

396 mean kinetic energy of the intermediate currents below 1000 m (Fig 9a), especially in the eastern

397 part of the basin (Fig 9b). Resolving the EICS results in similar results as what Getzlaff and Dietze

398 (2013) achieve with a simple parameterization of the EICS (Fig 9). To compensate for the

399 "missing" EICS in coarse resolution models, they enhanced anisotropically the lateral diffusivity in

400 the equatorial region. Implementing this approach tends to homogenize oxygen levels zonally,

401 with an increase of the mean levels by 30-50 mmol.m^{-3} in the eastern basin and a decrease of

402 oxygen concentrations in the western basin.

403

404 A possibly not intuitive feature is that the oxygen levels are relatively similar in GFDL025 and

405 GFDL1, while the current system is relatively similar in GFDL025 and GFDL01 (see Fig 5 and Fig

406 9). An explanation lies in the relatively small net balance between large fluxes of respiration and

407 oxygen supply (Duteil et al., 2014). If the supply is slightly higher compared to the consumption by
408 respiration, it will lead to an increase of oxygen concentration. If it is slightly lower, the oxygen
409 levels will decrease. A small difference in supply (e.g slightly weaker currents) may therefore lead
410 to a large difference in oxygen levels when integrated over decades. For this reason, the impact of
411 the EICS is more visible below 1000 m as the respiration decreases following a power-law with
412 depth (Martin et al., 1987) and is therefore easier to offset even by a moderate oxygen supply.
413

414 **5. Summary and conclusions**
415 Intermediate water masses (IWM) are subducted in the Southern Ocean and transported
416 equatorward to the tropics by isopycnal processes (Sloyan and Kamenkovich, 2007; Sallee et al.,
417 2013; Meijers, 2014). At lower latitudes they recirculate into the lower thermocline of the tropical
418 regions at 500 - 1500 m and into the EICS (Zenk et al., 2005; Marin et al., 2010; Cravatte et al.,
419 2012; 2017; Ascani et al., 2015; Menesguen et al., 2019) (see schema Fig 1). We show here that the
420 representation of this ventilation pathway is important to take into account when assessing tropical
421 oxygen levels and the extent of the OMZ in coupled biogeochemical circulation or climate models.
422 Particularly, we highlight two critical, yet typical, biases that hamper the correct representation of
423 the tropical oxygen levels.
424

425 5.1 Subducted IMW properties and tropical oxygen
426 First, the current generation of climate models, such as the CMIP5 models, show large deficiencies
427 in simulating IMW. Along with an unrealistic representation of IMW volume and properties when
428 the waters enter the subtropics, the models also lack the observed prominent oxygen maximum
429 associated with IMW. Restoring oxygen levels to observed concentrations at 30°S/30°N and at
430 1500 m depth in a coarse resolution model, comparable to CMIP5 climate models in terms of
431 resolution and oxygen bias, shows a significant impact on the lower thermocline (500 – 1500 m)
432 oxygen levels : a positive anomaly of 60 mmol.m^{-3} translates into an oxygen increase by 10 mmol-
433 m^{-3} in tropical regions after 50 years of integration.
434

435 The equatorward transport of the anomaly in the subtropics is mostly due to isopycnal subgrid scale
436 mixing processes as shown by the NEMO2 budget analysis. While the models with differing ocean
437 resolutions may differ in their transport of IWM between the subtropical regions and the tropics, it
438 nevertheless suggests that mesoscale activity in higher resolution models is important to spread
439 IWM (e.g Xu et al., 2016). This possibly includes subsurface eddies that show a signature well into
440 the IWM depth range (Frenger et al., 2018, see their Fig 2).

441

442 5.2 IMW transport and Equatorial Intermediate Current System

443 Second, the Equatorial Intermediate Current System (EICS) is not represented in coarse resolution

444 models and only poorly represented in high resolution ocean circulation models (0.25° and 0.1°), as

445 its strength remains too weak by a factor of two (consistent with previous studies, e.g Ascani et al.,

446 2015). The EICS transports the IWM that occupies the lower thermocline (500 – 1500 m depth) and

447 the recirculation of the IWM in the tropical ocean, as suggested by the observational study of Zenk

448 et al. (2005), and shown in our study.

449

450 We investigated the impact of the EICS on the oxygen supply with tracer release experiments: the

451 concentration of a conservative tracer that originates from the subtropical ocean, is, after 50 years,

452 30 % higher in the eastern equatorial (5°N-5S) Pacific in an ocean model with 0.1° resolution,

453 compared to an ocean model with 0.5 ° resolution. As the oxygen gradient along the equator is

454 similar to the gradient of the conservative tracer, we assume a similar enhancement of oxygen

455 supply by 30 % in the eastern equatorial Pacific at the same time scale. This means, if we account

456 for oxygen consumption due to respiration (about 1 $mmol.m^{-3}.yr^{-1}$ between 5°N-5°S, see section

457 3.2), that the better resolved EICS in the higher resolution ocean leads roughly to higher

458 intermediate oxygen levels of 15 - 30 $mmol-m^{-3}$ compared to the lower resolution ocean experiment

459 in a timescale of 50 years. Consistently, 0.1°-ocean GFDL01 model displays oxygen concentrations

460 larger by about 30 $mmol.m^{-3}$ in the eastern equatorial lower thermocline (500-1500 m) compared to

461 the 1°-ocean GFDL1 configuration (with higher subtropical oxygen concentrations of IWM of 15

462 $mmol.m^{-3}$ in GFDL01 at 30°S)

463

464 We would like to highlight two potential implications of our finding of the important role of the

465 EICS for the Pacific eastern tropical oxygen supply: i) First, we have shown that the intermediate

466 current system EICS is important for the connection between the western and eastern Pacific Ocean

467 at a decadal / multidecadal time scale. This suggests that the EICS modulates the mean state and the

468 variability of the tropical oxygen in the lower thermocline, and subsequently the whole water

469 column by upwelling of deep waters. ii) Second, we have found an enhancement of the connections

470 between equatorial deep ocean (> 2000 m) and lower thermocline in the high resolution model

471 compared to the lower resolution model. This result is consistent with the studies of Brandt et al.

472 (2011, 2012), who suggested, based on observational data and on an idealized model, that

473 Equatorial Deep Jets, part of the EICS (see Fig 1b), propagate their energy upward and impact the

474 upper ocean properties of the ocean, including their oxygen content. Taken this into account, we

475 hypothesize that the Pacific Deep Water has a larger role than previously thought in modulating the

476 intermediate and upper ocean properties.

477

478 A pragmatic approach to account for the missing EICS is to increase diffusion anisotropically, with

479 increased zonal mixing in the tropics (Getzlaff and Dietze, 2013). This parameterization mimics a

480 more vigorous EICS and improves the simulated shape of the OMZ in climate models. However,

481 the prominent bias of IMW in climate models, and therefore of the water masses entering the EICS

482 is not accounted for with this parameterization. Furthermore such a parameterization improves the

483 mean state but does not reproduce the variability of the EICS.

484

485 5.3 Implication for biogeochemical cycles

486 The IWM are important supplier of oxygen to the tropical oceans, but also of nutrients (Palter et al.,

487 2010) as well as anthropogenic carbon (e.g Kathiwala et al., 2012), which accumulates in mode and

488 intermediate waters of the Southern Ocean (Sabine et al., 2004; Resplandy et al., 2013). The

489 mechanisms that we discussed here may therefore play a role in ocean carbon climate feedbacks on

490 time scales of decades to a century.

491

492 Finally, this study suggests that changes of the properties of the IWM may contribute to the still

493 partly unexplained deoxygenation of 5 mmol.m^{-3} / decade occuring in the lower thermocline of the

494 equatorial eastern Pacific Ocean (Schmidtko et al., 2017; Oschlies et al., 2018). In addition to an

495 oxygen decrease in tropical regions, Schmidtko et al. (2017) showed a decrease of oxygen levels by

496 2-5 mmol.m^{-3} in the regions of formations of AAIW. Based on repeated cruise observations,

497 Panassa et al. (2018) highlighted an increase of the apparent oxygen utilization in the core of the

498 AAIW, related to a 5 % increase in nutrient concentrations from 1990 to 2014. The transport of this

499 modified AAIW, poorer in oxygen and richer in nutrients, toward the low latitudes both by small

500 scale processes (section 3) and at the equator by the EICS (section 4), may explain a significant part

501 of the occuring deoxygenation in the equatorial ocean. In complement to changes in the AAIW

502 properties, little is known about the variability and long term trend of the strength of the EICS, an

503 oceanic "bridge" between the western and the eastern part of the basin. A possible way forward

504 could be to perform idealized model experiments in high resolution configurations, aiming to assess

505 both the effect of the observed change in the AAIW properties and of a potential change of EICS

506 strength on oxygen levels.

507

508

Data and code availability

The code for the Nucleus for European Modeling of the Ocean (NEMO) is available at: https://www.nemo-ocean.eu/. The code for the University of Victoria (UVIC) model is available at :http://terra.seos.uvic.ca/model/. The Lagrangian particles ARIANE code is available at http://stockage.univ-brest.fr/~grima/Ariane/. The Coordinated Ocean-ice Reference Experiments (COREv2) dataset is available at: https://data1.gfdl.noaa.gov/nomads/forms/core/COREv2.html. The experiments data is available on request.

Authors contributions

OD conceived the study, performed the NEMO model and ARIANE experiments and analyzed the data. IF preprocessed and helped to analyze the GFDL data. JG preprocessed and helped to analyze the UVIC data. All authors discussed the results and wrote the manuscript.

Competing interest

The authors declare that they have no conflict of interest.

Acknowledgments

This work is a contribution of the SFB754 "Climate-Biogeochemistry Interactions in the Tropical Ocean", supported by the Deutsche Forschungsgemeinschaft (DFG). The NEMO simulations were performed at the North German Supercomputing Alliance (HLRN). We would like to thank Markus Scheinert (research unit "Ocean Dynamics", GEOMAR) for his technical support in compiling the NEMO code and for providing the high resolution NEMO input files. We would like to thank GFDL for producing the CM2-0 suite that involved a substantial commitment of computational resources and data storage.

542 **References**

543 Ascani, F., Firing, E., Dutrieux, P., McCreary, J. P., & Ishida, A. (2010). Deep Equatorial Ocean

544 Circulation Induced by a Forced–Dissipated Yanai Beam. Journal of Physical Oceanography, 40(5),

545 1118–1142. doi:10.1175/2010jpo4356.1

546 Ascani, F., Firing, E., McCreary, J. P., Brandt, P., & Greatbatch, R. J. (2015). The Deep Equatorial

547 Ocean Circulation in Wind-Forced Numerical Solutions. Journal of Physical Oceanography, 45(6),

548 1709–1734. doi:10.1175/jpo-d-14-0171.1

549 Bahl, A., Gnanadesikan, A., & Pradal, M. A. (2019). Variations in Ocean Deoxygenation Across

550 Earth System Models: Isolating the Role of Parameterized Lateral Mixing. Global Biogeochemical

551 Cycles, 33(6), 703–724. doi:10.1029/2018gb006121

552 Blanke, B., & Raynaud, S. (1997). Kinematics of the Pacific Equatorial Undercurrent: An Eulerian

553 and Lagrangian Approach from GCM Results. Journal of Physical Oceanography, 27(6), 1038–

554 1053. doi:10.1175/1520-0485(1997)027<1038:kotpeu>2.0.co;2

555 Brandt, P., Funk, A., Hormann, V., Dengler, M., Greatbatch, R. J., & Toole, J. M. (2011).

556 Interannual atmospheric variability forced by the deep equatorial Atlantic Ocean. Nature,

557 473(7348), 497–500. doi:10.1038/nature10013

558 Brandt, P., Greatbatch, R. J., Claus, M., Didwischus, S.-H., Hormann, V., Funk, A., … Körtzinger,

559 A. (2012). Ventilation of the equatorial Atlantic by the equatorial deep jets. Journal of Geophysical

560 Research: Oceans, 117(C12), n/a–n/a. doi:10.1029/2012jc008118

561 Breitburg, D., Levin, L. A., Oschlies, A., Grégoire, M., Chavez, F. P., Conley, D. J., … Zhang, J.

562 (2018). Declining oxygen in the global ocean and coastal waters. Science, 359(6371), eaam7240.

563 doi:10.1126/science.aam7240

564 Busecke, J. J. M., Resplandy, L., & Dunne, J. P. (2019). The Equatorial Undercurrent and the

565 Oxygen Minimum Zone in the Pacific. Geophysical Research Letters, 46(12), 6716–6725.

566 doi:10.1029/2019gl082692

567 Cabré, A., Marinov, I., Bernardello, R., & Bianchi, D. (2015). Oxygen minimum zones in the

568 tropical Pacific across CMIP5 models: mean state differences and climate change trends.

569 Biogeosciences, 12(18), 5429–5454. doi:10.5194/bg-12-5429-2015

570 Carrasco, C., Karstensen, J., & Farias, L. (2017). On the Nitrous Oxide Accumulation in

571 Intermediate Waters of the Eastern South Pacific Ocean. Frontiers in Marine Science, 4.

572 doi:10.3389/fmars.2017.00024

573 Cravatte, S., Kessler, W. S., & Marin, F. (2012). Intermediate Zonal Jets in the Tropical Pacific

574 Ocean Observed by Argo Floats. Journal of Physical Oceanography, 42(9), 1475–1485.

575 doi:10.1175/jpo-d-11-0206.1

576   Cravatte, S., Kestenare, E., Marin, F., Dutrieux, P., & Firing, E. (2017). Subthermocline and

577   Intermediate Zonal Currents in the Tropical Pacific Ocean: Paths and Vertical Structure. Journal of

578   Physical Oceanography, 47(9), 2305–2324. doi:10.1175/jpo-d-17-0043.1

579   Czeschel, R., Stramma, L., Schwarzkopf, F. U., Giese, B. S., Funk, A., and Karstensen, J. (2011),

580   Middepth circulation of the eastern tropical South Pacific and its link to the oxygen minimum zone,

581   J. Geophys. Res., 116, C01015, doi:10.1029/2010JC006565

582   Delworth, T. L., Rosati, A., Anderson, W., Adcroft, A. J., Balaji, V., Benson, R., … Zhang, R.

583   (2012). Simulated Climate and Climate Change in the GFDL CM2.5 High-Resolution Coupled

584   Climate Model. Journal of Climate, 25(8), 2755–2781. doi:10.1175/jcli-d-11-00316.1

585   Dietze, H., & Loeptien, U. (2013). Revisiting "nutrient trapping" in global coupled biogeochemical

586   ocean circulation models. Global Biogeochemical Cycles, 27(2), 265–284. doi:10.1002/gbc.20029

587   Dufour, C. O., Griffies, S. M., de Souza, G. F., Frenger, I., Morrison, A. K., Palter, J. B., … Slater,

588   R. D. (2015). Role of Mesoscale Eddies in Cross-Frontal Transport of Heat and Biogeochemical

589   Tracers in the Southern Ocean. Journal of Physical Oceanography, 45(12), 3057–3081. doi:10.1175/

590   jpo-d-14-0240.1

591   Duteil, O., & Oschlies, A. (2011). Sensitivity of simulated extent and future evolution of marine

592   suboxia to mixing intensity. Geophysical Research Letters, 38(6), n/a–n/a.

593   doi:10.1029/2011gl046877

594   Duteil, O., Koeve, W., Oschlies, A., Aumont, O., Bianchi, D., Bopp, L., … Segschneider, J. (2012).

595   Preformed and regenerated phosphate in ocean general circulation models: can right total

596   concentrations be wrong? Biogeosciences, 9(5), 1797–1807. doi:10.5194/bg-9-1797-2012

597   Duteil, O., Böning, C. W., & Oschlies, A. (2014). Variability in subtropical-tropical cells drives

598   oxygen levels in the tropical Pacific Ocean. Geophysical Research Letters, 41(24), 8926–8934.

599   doi:10.1002/2014gl061774

600   Duteil, O., Oschlies, A., & Böning, C. W. (2018). Pacific Decadal Oscillation and recent oxygen

601   decline in the eastern tropical Pacific Ocean. Biogeosciences, 15(23), 7111–7126. doi:10.5194/bg-

602   15-7111-2018

603   Duteil, O. (2019). Wind Synoptic Activity Increases Oxygen Levels in the Tropical Pacific Ocean.

604   Geophysical Research Letters, 46(5), 2715–2725. doi:10.1029/2018gl081041

605   Eden, C., & Dengler, M. (2008). Stacked jets in the deep equatorial Atlantic Ocean. Journal of

606   Geophysical Research, 113(C4). doi:10.1029/2007jc004298

607   Firing, E., Wijffels, S. E., & Hacker, P. (1998). Equatorial subthermocline currents across the

608   Pacific. Journal of Geophysical Research: Oceans, 103(C10), 21413–21423. doi:10.1029/98jc01944

609   Firing, E. (1987). Deep zonal currents in the central equatorial Pacific. Journal of Marine Research,

610   45(4), 791–812. doi:10.1357/002224087788327163

611   Frenger, I., Bianchi, D., Stührenberg, C., Oschlies, A., Dunne, J., Deutsch, C., … Schütte, F.

612   (2018). Biogeochemical Role of Subsurface Coherent Eddies in the Ocean: Tracer Cannonballs,

613   Hypoxic Storms, and Microbial Stewpots? Global Biogeochemical Cycles, 32(2), 226–249.

614   doi:10.1002/2017gb005743

615   Galbraith, E. D., Dunne, J. P., Gnanadesikan, A., Slater, R. D., Sarmiento, J. L., Dufour, C. O., …

616   Marvasti, S. S. (2015). Complex functionality with minimal computation: Promise and pitfalls of

617   reduced-tracer ocean biogeochemistry models. Journal of Advances in Modeling Earth Systems,

618   7(4), 2012–2028. doi:10.1002/2015ms000463

619   Getzlaff, J., & Dietze, H. (2013). Effects of increased isopycnal diffusivity mimicking the

620   unresolved equatorial intermediate current system in an earth system climate model. Geophysical

621   Research Letters, 40(10), 2166–2170. doi:10.1002/grl.50419

622   Gnanadesikan, A., Bianchi, D., & Pradal, M. (2013). Critical role for mesoscale eddy diffusion in

623   supplying oxygen to hypoxic ocean waters. Geophysical Research Letters, 40(19), 5194–5198.

624   doi:10.1002/grl.50998

625   Gouriou, Y., Delcroix, T., & Eldin, G. (2006). Upper and intermediate circulation in the western

626   equatorial Pacific Ocean in October 1999 and April 2000. Geophysical Research Letters, 33(10), n/

627   a–n/a. doi:10.1029/2006gl025941

628   Griffies, S. M., Winton, M., Anderson, W. G., Benson, R., Delworth, T. L., Dufour, C. O., …

629   Zhang, R. (2015). Impacts on Ocean Heat from Transient Mesoscale Eddies in a Hierarchy of

630   Climate Models. Journal of Climate, 28(3), 952–977. doi:10.1175/jcli-d-14-00353.1

631   Iudicone, D., Rodgers, K. B., Schopp, R., & Madec, G. (2007). An Exchange Window for the

632   Injection of Antarctic Intermediate Water into the South Pacific. Journal of Physical Oceanography,

633   37(1), 31–49. doi:10.1175/jpo2985.1

634   Izumo, T. (2005). The equatorial undercurrent, meridional overturning circulation, and their roles in

635   mass and heat exchanges during El Niño events in the tropical Pacific ocean. Ocean Dynamics,

636   55(2), 110–123. doi:10.1007/s10236-005-0115-1

637   Khatiwala, S., Tanhua, T., Mikaloff Fletcher, S., Gerber, M., Doney, S. C., Graven, H. D., …

638   Sabine, C. L. (2013). Global ocean storage of anthropogenic carbon. Biogeosciences, 10(4), 2169–

639   2191. doi:10.5194/bg-10-2169-2013

640   Kawabe, M., & Fujio, S. (2010). Pacific ocean circulation based on observation. Journal of

641   Oceanography, 66(3), 389–403. doi:10.1007/s10872-010-0034-8

642 Keller, D. P., Oschlies, A., & Eby, M. (2012). A new marine ecosystem model for the University of

643 Victoria Earth System Climate Model. Geoscientific Model Development, 5(5), 1195–1220.

644 doi:10.5194/gmd-5-1195-2012

645 Koshlyakov, M.N. and Tarakanov, R.Y. (2003). Antarctic Bottom Water in the Pacific sector of the

646 Southern Ocean, Oceanology 43(1):1-15

647 Kriest, I., Khatiwala, S., & Oschlies, A. (2010). Towards an assessment of simple global marine

648 biogeochemical models of different complexity. Progress in Oceanography, 86(3-4), 337–360.

649 doi:10.1016/j.pocean.2010.05.002

650 Lachkar, Z., Orr, J. C., & Dutay, J.-C. (2009). Seasonal and mesoscale variability of oceanic

651 transport of anthropogenic CO2. Biogeosciences, 6(11), 2509–2523. doi:10.5194/bg-6-2509-2009

652 Large, W. G., & Yeager, S. G. (2008). The global climatology of an interannually varying air–sea

653 flux data set. Climate Dynamics, 33(2-3), 341–364. doi:10.1007/s00382-008-0441-3

654 Lübbecke, J. F., Böning, C. W., & Biastoch, A. (2008). Variability in the subtropical-tropical cells

655 and its effect on near-surface temperature of the equatorial Pacific: a model study. Ocean Science,

656 4(1), 73–88. doi:10.5194/os-4-73-2008

657 Gurvan, M., Bourdallé-Badie, R., Pierre-Antoine Bouttier, Bricaud, C., Bruciaferri, D., Calvert, D.,

658 Chanut, J., Clementi, E., Coward, A., Delrosso, D., Ethé, C., Flavoni, S., Graham, T., Harle, J.,

659 Iovino, D., Lea, D., Lévy, C., Lovato, T., Martin, N., … Vancoppenolle, M. (2017). <i>NEMO

660 ocean engine</i>. https://doi.org/10.5281/ZENODO.3248739Marin, F., Kestenare, E., Delcroix, T.,

661 Durand, F., Cravatte, S., Eldin, G., & Bourdallé-Badie, R. (2010). Annual Reversal of the

662 Equatorial Intermediate Current in the Pacific: Observations and Model Diagnostics. Journal of

663 Physical Oceanography, 40(5), 915–933. doi:10.1175/2009jpo4318.1

664 Martin, J. H., Knauer, G. A., Karl, D. M., & Broenkow, W. W. (1987). VERTEX: carbon cycling in

665 the northeast Pacific. Deep Sea Research Part A. Oceanographic Research Papers, 34(2), 267–285.

666 doi:10.1016/0198-0149(87)90086-0

667 Meijers, A. J. S. (2014). The Southern Ocean in the Coupled Model Intercomparison Project phase

668 5. Philosophical Transactions of the Royal Society A: Mathematical, Physical and Engineering

669 Sciences, 372(2019), 20130296. doi:10.1098/rsta.2013.0296

670 Ménesguen, C., Delpech, A., Marin, F., Cravatte, S., Schopp, R., & Morel, Y. (2019). Observations

671 and Mechanisms for the Formation of Deep Equatorial and Tropical Circulation. Earth and Space

672 Science, 6(3), 370–386. doi:10.1029/2018ea000438

673 Molinelli EJ (1981) The Antarctic influence on Antarctic Intermediate Water. J Mar Res 39:267–

674 293

675 Oschlies, A., Brandt, P., Stramma, L., & Schmidtko, S. (2018). Drivers and mechanisms of ocean

676 deoxygenation. Nature Geoscience, 11(7), 467–473. doi:10.1038/s41561-018-0152-2

677 Palter, J. B., Sarmiento, J. L., Gnanadesikan, A., Simeon, J., and Slater, R. D. (2010). Fueling

678 export production: nutrient return pathways from the deep ocean and their dependence on the

679 Meridional Overturning Circulation, Biogeosciences, 7, 3549–3568, doi:10.5194/bg-7-3549-2010

680 Panassa, E., Santana-Casiano, J. M., González-Dávila, M., Hoppema, M., van Heuven, S. M. A. .,

681 Völker, C., … Hauck, J. (2018). Variability of nutrients and carbon dioxide in the Antarctic

682 Intermediate Water between 1990 and 2014. Ocean Dynamics, 68(3), 295–308.

683 doi:10.1007/s10236-018-1131-2

684 Pardo, P. C., Pérez, F. F., Velo, A., & Gilcoto, M. (2012). Water masses distribution in the Southern

685 Ocean: Improvement of an extended OMP (eOMP) analysis. Progress in Oceanography, 103, 92–

686 105. doi:10.1016/j.pocean.2012.06.002

687 Paulmier, A., Ruiz-Pino (2009), D. Oxygen minimum zones (OMZs) in the modern ocean,Progress

688 in Oceanography, 80(3), 113-128, doi:10.1016/j.pocean.2008.08.001.

689 Qu, T., & Lindstrom, E. J. (2004). Northward Intrusion of Antarctic Intermediate Water in the

690 Western Pacific*. Journal of Physical Oceanography, 34(9), 2104–2118. doi:10.1175/1520-

691 0485(2004)034<2104:nioaiw>2.0.co;2

692 Resplandy, L., Bopp, L., Orr, J. C., & Dunne, J. P. (2013). Role of mode and intermediate waters in

693 future ocean acidification: Analysis of CMIP5 models. Geophysical Research Letters, 40(12),

694 3091–3095. doi:10.1002/grl.50414

695 Rowe, G. D., Firing, E., & Johnson, G. C. (2000). Pacific Equatorial Subsurface Countercurrent

696 Velocity, Transport, and Potential Vorticity*. Journal of Physical Oceanography, 30(6), 1172–1187.

697 doi:10.1175/1520-0485(2000)030<1172:pescvt>2.0.co;2

698 Russell, J. L., & Dickson, A. G. (2003). Variability in oxygen and nutrients in South Pacific

699 Antarctic Intermediate Water. Global Biogeochemical Cycles, 17(2), n/a–n/a.

700 doi:10.1029/2000gb001317

701 Sabine, C. L. (2004). The Oceanic Sink for Anthropogenic CO2. Science, 305(5682), 367–371.

702 doi:10.1126/science.1097403

703 Sallée, J.-B., Shuckburgh, E., Bruneau, N., Meijers, A. J. S., Bracegirdle, T. J., Wang, Z., & Roy, T.

704 (2013). Assessment of Southern Ocean water mass circulation and characteristics in CMIP5

705 models: Historical bias and forcing response. Journal of Geophysical Research: Oceans, 118(4),

706 1830–1844. doi:10.1002/jgrc.20135

707 Schmidtko, S., Stramma, L., & Visbeck, M. (2017). Decline in global oceanic oxygen content

708 during the past five decades. Nature, 542(7641), 335–339. doi:10.1038/nature21399

709 Sen Gupta, A., & England, M. H. (2007). Evaluation of Interior Circulation in a High-Resolution

710 Global Ocean Model. Part II: Southern Hemisphere Intermediate, Mode, and Thermocline Waters.

711 Journal of Physical Oceanography, 37(11), 2612–2636. doi:10.1175/2007jpo3644.1

712 Shigemitsu, M., Yamamoto, A., Oka, A., & Yamanaka, Y. (2017). One possible uncertainty in

713 CMIP5 projections of low-oxygen water volume in the Eastern Tropical Pacific. Global

714 Biogeochemical Cycles, 31(5), 804–820. doi:10.1002/2016gb005447

715 Sloyan, B. M., & Kamenkovich, I. V. (2007). Simulation of Subantarctic Mode and Antarctic

716 Intermediate Waters in Climate Models. Journal of Climate, 20(20), 5061–5080.

717 doi:10.1175/jcli4295.1

718 Sloyan, B. M., & Rintoul, S. R. (2001). Circulation, Renewal, and Modification of Antarctic Mode

719 and Intermediate Water*. Journal of Physical Oceanography, 31(4), 1005–1030. doi:10.1175/1520-

720 0485(2001)031<1005:cramoa>2.0.co;2

721 Takano, Y., Ito, T., & Deutsch, C. (2018). Projected Centennial Oxygen Trends and Their

722 Attribution to Distinct Ocean Climate Forcings. Global Biogeochemical Cycles, 32(9), 1329–1349.

723 doi:10.1029/2018gb005939

724 Talley, L. D. (1993). Distribution and Formation of North Pacific Intermediate Water. Journal of

725 Physical Oceanography, 23(3), 517–537. doi:10.1175/1520-0485(1993)023<0517:dafonp>2.0.co;2

726 Weaver, A. J., Eby, M., Wiebe, E. C., Bitz, C. M., Duffy, P. B., Ewen, T. L., … Yoshimori, M.

727 (2001). The UVic earth system climate model: Model description, climatology, and applications to

728 past, present and future climates. Atmosphere-Ocean, 39(4), 361–428.

729 doi:10.1080/07055900.2001.9649686

730 Xu, L., Li, P., Xie, S. et al. (2016). Observing mesoscale eddy effects on mode-water subduction

731 and transport in the North Pacific. Nature Communications, 10505 (2016),

732 doi.org/10.1038/ncomms10505

733 Zenk, W., Siedler, G., Ishida, A., Holfort, J., Kashino, Y., Kuroda, Y., … Müller, T. J. (2005).

734 Pathways and variability of the Antarctic Intermediate Water in the western equatorial Pacific

735 Ocean. Progress in Oceanography, 67(1-2), 245–281. doi:10.1016/j.pocean.2005.05.003

736 Zhu, C., Liu, Z., & Gu, S. (2017). Model bias for South Atlantic Antarctic intermediate water in

737 CMIP5. Climate Dynamics, 50(9-10), 3613–3624. doi:10.1007/s00382-017-3828-1

738

739

740

741

742

Table and Figures

Table 1 :

Model	Resolution	Atmosphere	BGC	Model Reference (circulation)	Model Reference (BGC)
Mean state comparison					
UVIC	2.8°	Coupled (temperature, humidity) Forced (NCEP/NCAR wind stress)	UVIC-BGC	Weaver et al., 2001	Keller et al., 2012
NEMO2	2° (0.5 eq)	Forced COREv2 "normal year"	NPZD-O2	Madec et al., 2017	Kriest et al, 2010 Duteil et al., 2014
GFDL1	1°	Coupled (~50 km)	miniBLING	Delworth et al, 2012, Griffies et al, 2015	Galbraith et al., 2015, Dufour et al, 2015
GFDL025	0.25 °	Coupled (~50 km)	miniBLING		
GFDL01	0.1°	Coupled (~50 km)	miniBLING		
Sensitivity experiments					
Model	Resolution	Atmosphere	BGC	Experiments	
NEMO2 (section 2.2.1)	2° (0.5 eq)	Forced COREv2 1948-2007	NPZD-O2	REF: control experiment 30N30S: O2 restoring to WOA at 30°N/30°S 30N30S1500M: O2 restoring to WOA at 30°N/30°S/1500m	
NEMO05 (section 2.2.2)	0.5°	Forced COREv2 1948 - 2007	Tracer release	Tracer initialized to 1 (O2 WOA > 150 mmol.m^{-3}) or 0 (O2 WOA < 150 mmol-m-3)	
NEMO01 (section 2.2.2)	0.1°	Forced COREv2 1948 – 2007	Tracer release		

753
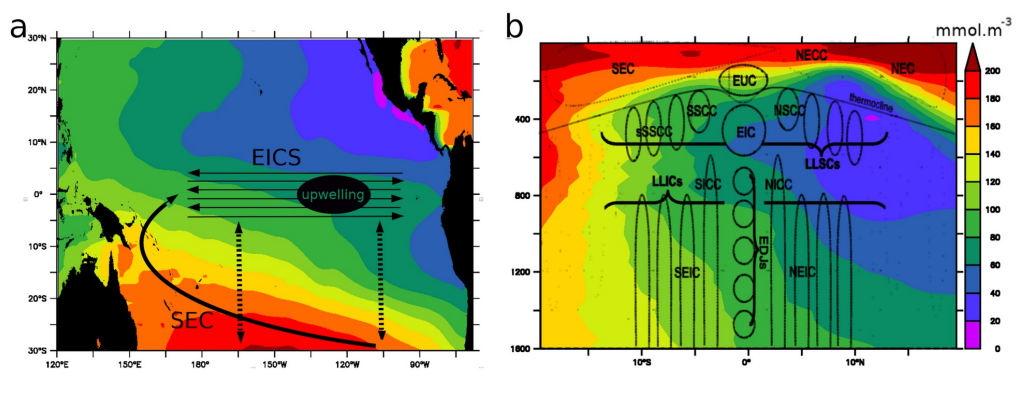
754

755

756

757 Figure 1 : a- schema summarizing the intermediate water masses (IWM) pathway from the

758 subtropics into the equatorial regions. EICS : Equatorial Intermediate Current System. SEC : South

759 Equatorial Current. Dashed line : isopycnal diffusive processes. Oxygen levels (mmol.m^{-3}) in the

760 lower thermocline (mean 500-1500m) are represented in color. b - schema (adapted from

761 Menesguen et al., 2019) illustrating the complexity of the EICS, extending below the thermocline

762 till more than 2000 m depth (see section 4.1 for a detailed description). Oxygen levels (mean 500 –

763 1500m) at 160°W are represented in color (mmol.m^{-3}).
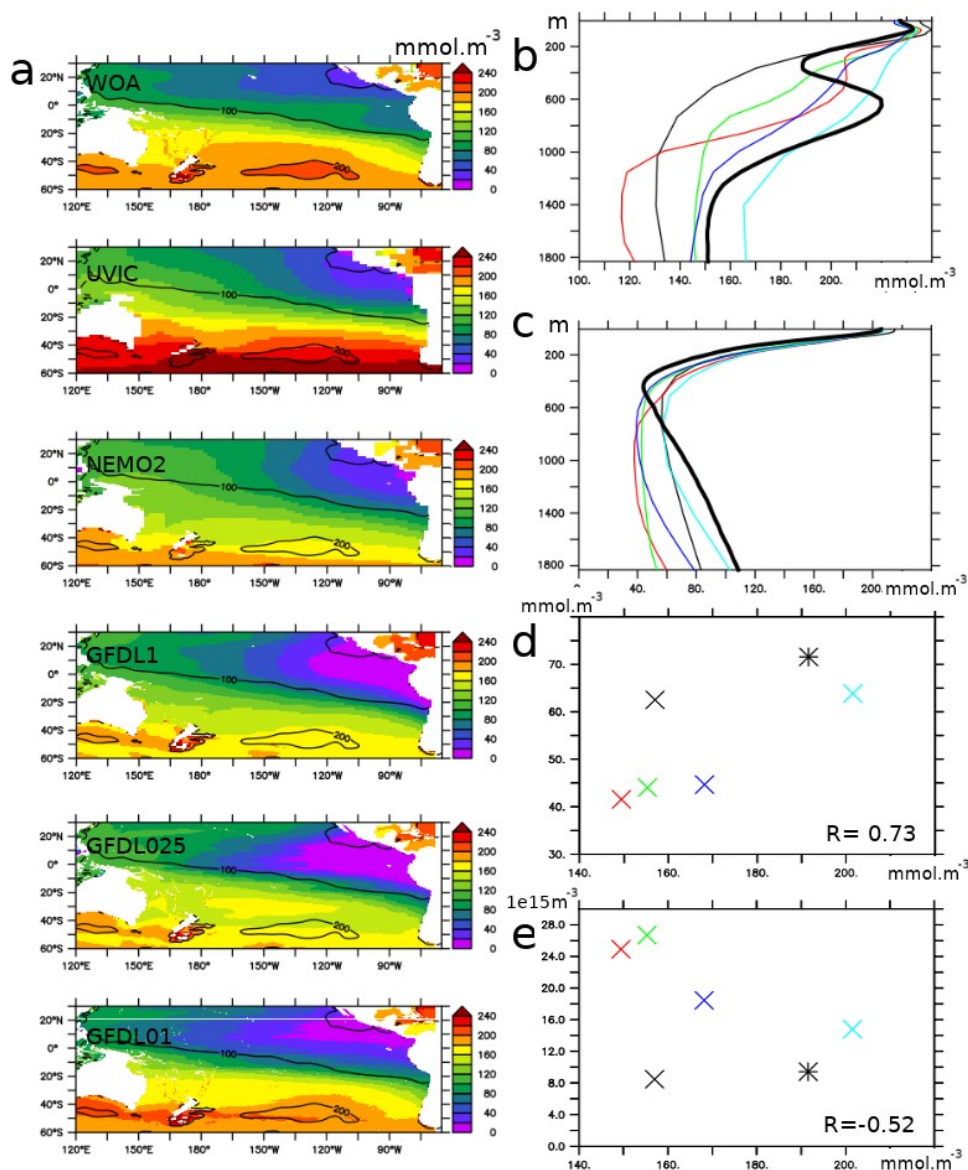
Figure 2 : a- oxygen levels (mmol.m^{-3}) in observations (World Ocean Atlas - WOA) (mean 500 – 1500 m) and models (UVIC, NEMO2, GFDL1, GFDL025, GFDL01). Contours correspond to WOA values. b: average "30°S" (120°E-65°W, 30°S) c : average "tropics" (160°W-coast, 20°N-20°S). d: average "30°S" vs "tropics". e: average "30°S" vs volume of tropical suboxic ocean (oxygen lower than 20 mmol.m^{-3}) regions (1e15m3). UVIC : black, NEMO2 : cyan, GFDL1 : red, GFDL025, green; GFDL01 : blue, WOA: star.

771

772

773

774
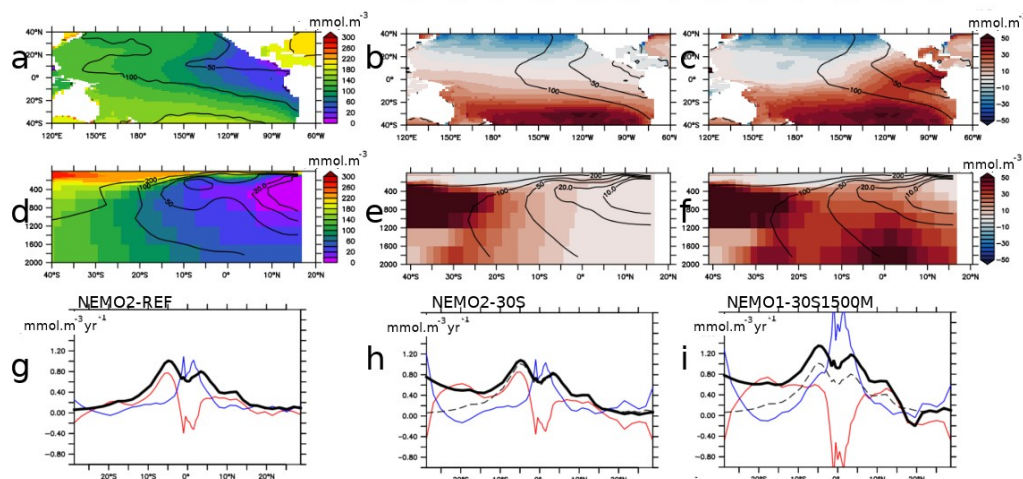
Figure 3 : a- Oxygen (mmol.m^{-3}) in the experiments NEMO2-REF (color) and World Ocean Atlas (contour) (average 500-1500 m). b- Oxygen (mmol.m^{-3}) difference (average 500 - 1500 m) between the experiments NEMO2-30S minus NEMO2-REF and c- NEMO2-30S1500M minus NEMO2-REF (contour NEMO2-REF). d- Oxygen (mmol.m^{-3}) in the experiments NEMO2-REF (color) and World Ocean Atlas (contour) (100°W). e- Oxygen (mmol.m^{-3}) difference (100°W) between the experiments NEMO2-30S minus NEMO2-REF and f- NEMO2-30S1500M minus NEMO2-REF (contour NEMO2-REF). g-i : basin zonal average (average 500 - 1500 m) of the oxygen total supply (bold) (mmol.m^{-3}.year^{-1}), advective processes (blue) and isopycnal diffusion (red) in g - NEMO2-REF, h- NEMO2-30DEG, i-NEMO2-30DEG1500M. The dashed line in is the oxygen total supply in NEMO2-REF.

785
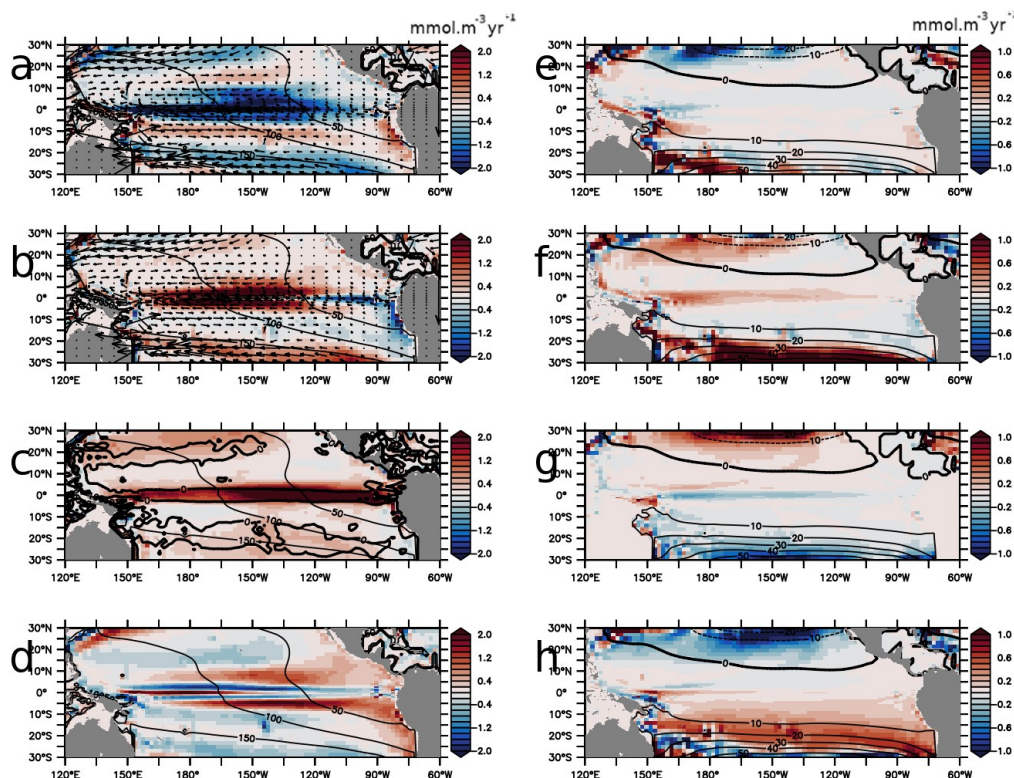
Figure 4 : Oxygen supply processes (mmol.m⁻³.year⁻¹ – average 500 - 1500m) in NEMO2-REF : a-
zonal advection, b– meridional advection, c- vertical advection, d- isopycnal diffusion. The
meridional and zonal currents are displayed as vectors in a,b and the vertical current as contour in c.
Oxygen levels (mmol-m.⁻³) are displayed in contour. Difference in oxygen supply processes
(mmol.m⁻³.year⁻¹ – average 500-1500m) between NEMO2-30DEG and NEMO2-REF : e- zonal
advection, f – meridional advection, g- vertical advection, h- isopycnal diffusion. The NEMO2-
30DEG – NEMO2-REF oxygen anomaly (mmol.m⁻³) is displayed in contour.

794
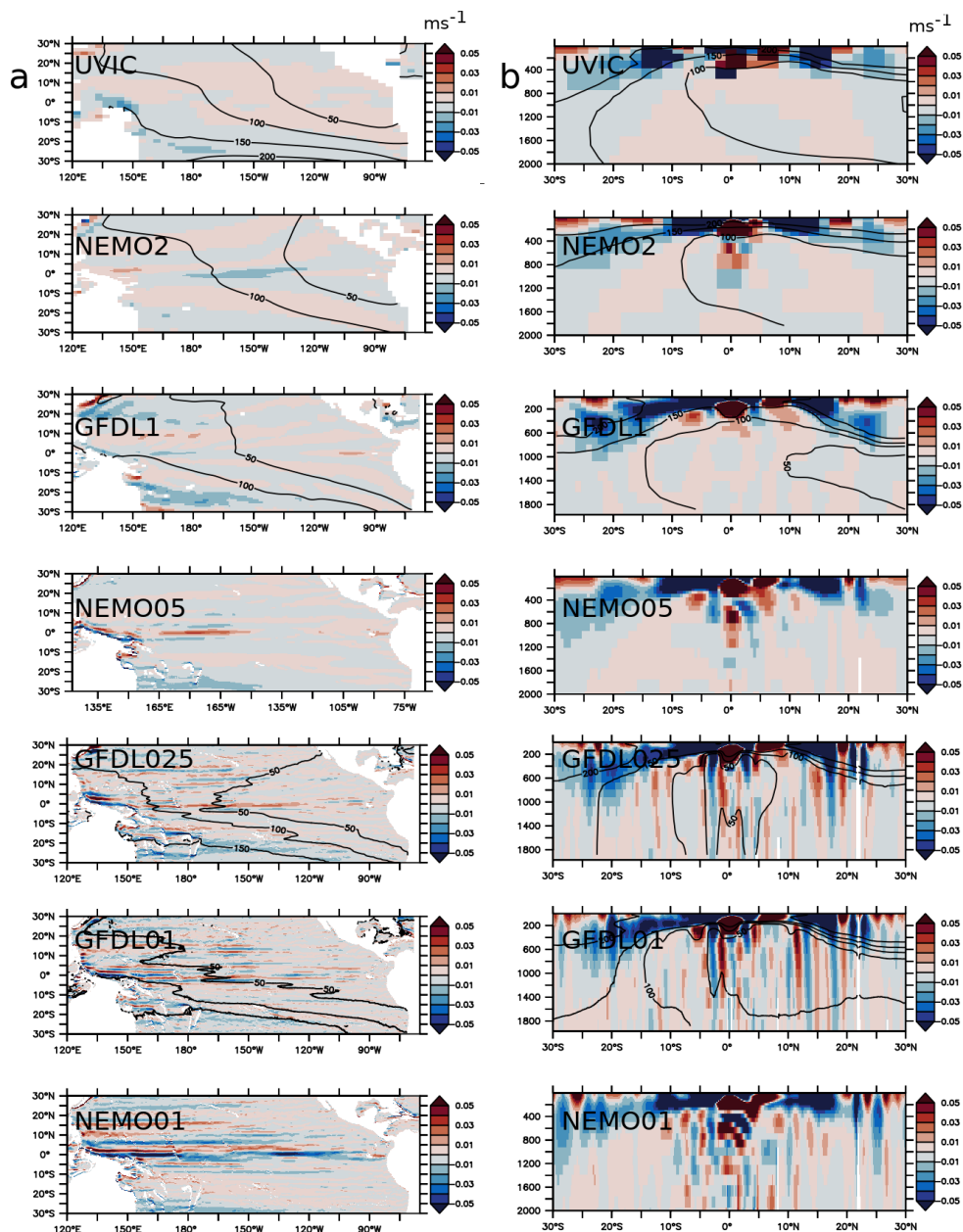
Figure 5 : mean currents velocity (ms^{-1}) at a- 1000 m depth   b- 100°W in UVIC, NEMO2,

NEMO05, GFDL025, GFDL01, NEMO01. The mean oxygen levels (mmol.m^{-3}) (when coupled

circulation-biogeochemical experiments have been performed – see Table 1) are displayed in

contour

799
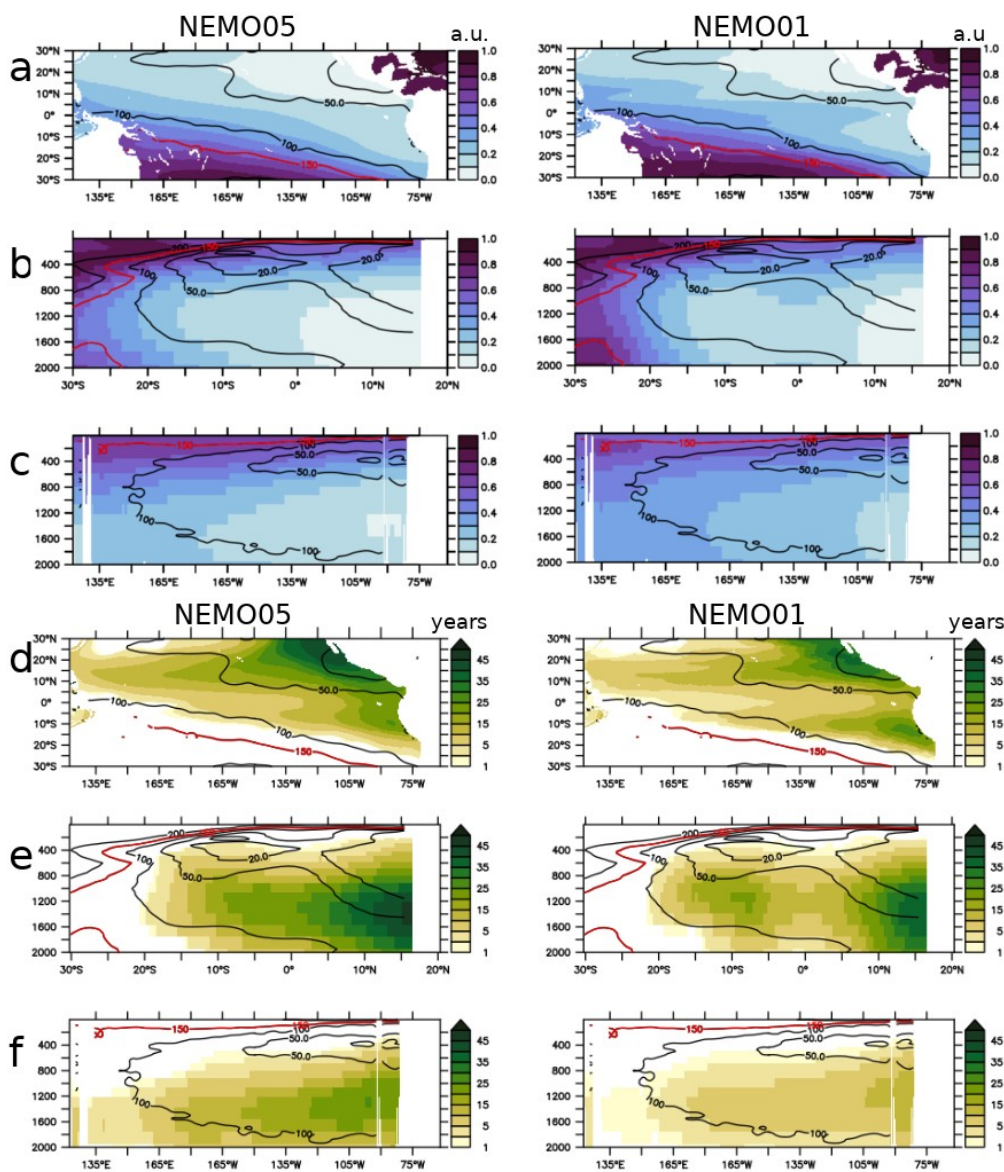
Figure 6: a-c : tracer concentration (arbitrary unit) after 60 years integration in NEMO05 (left) and NEMO01 (right). a- average 500-1500m, b- section 100°W, c- equatorial section. d-f: Time (years) at which the released tracer reaches the concentration 0.1 (t10%) in NEMO05 and NEMO01. d- average 500-1500m, e- section 100°W, f- equatorial section. In all the subpanels, the WOA oxygen levels are displayed in contour. The red contour is the WOA 150 mmol.m^{-3} oxygen isoline, used to initialize the tracer level.

806

807
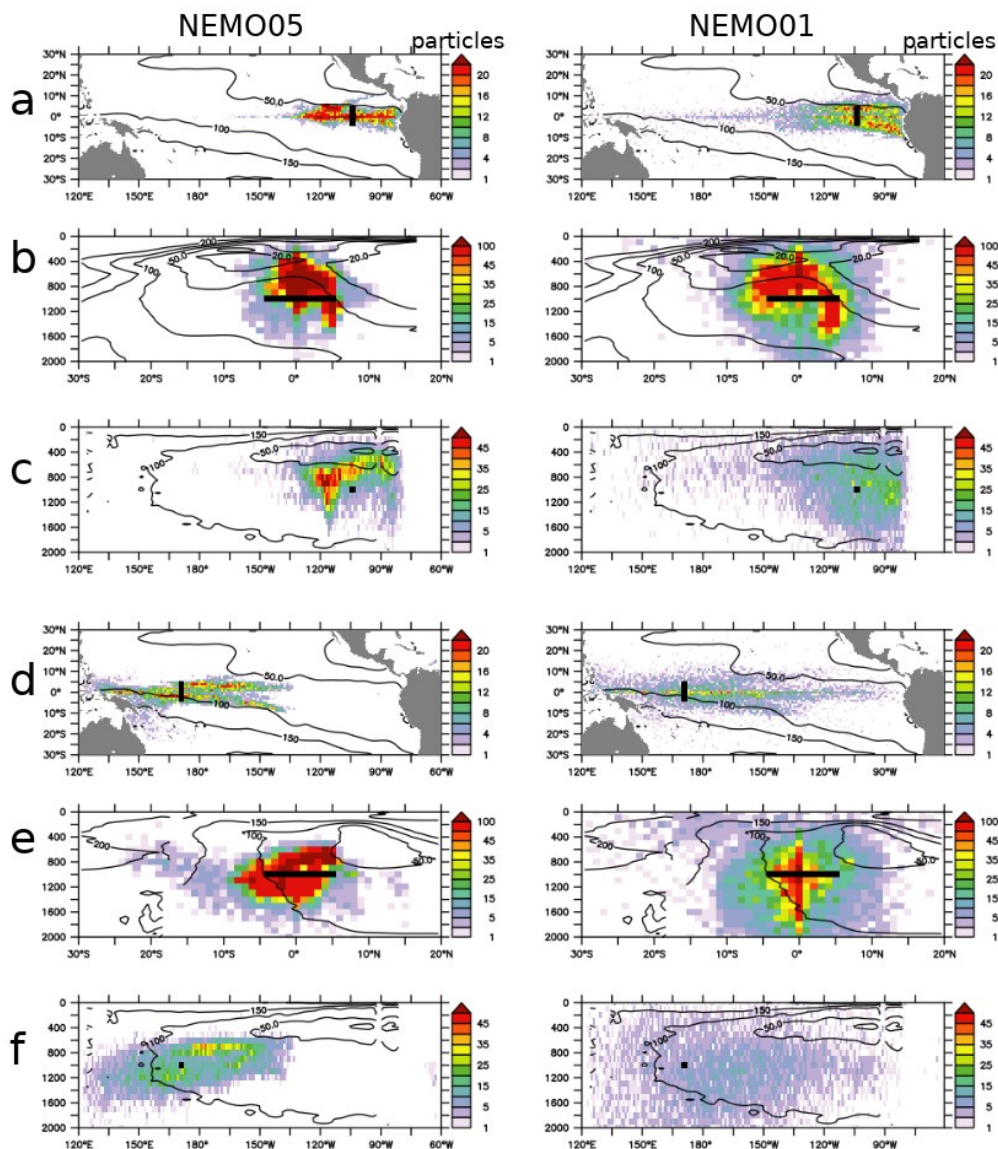
Figure 7 : Density (number of particles in a 1°x1°x100m depth box) distribution of the location of released Lagrangian particles (15 years backward integration starting from the final experiment state) in NEMO05 (left) and NEMO01 (right). The release location is identified in bold and is located at 100°W/5°N-5S/1000 m depth. a- vertical integrated density; b- zonal integrated density; c- meridional integrated density. d-f : Similar to a-c but with a release location located at 160°E/5°N-5°S/1000 m depth. The mean oxygen levels are displayed in contour.

814

815

816

817

818
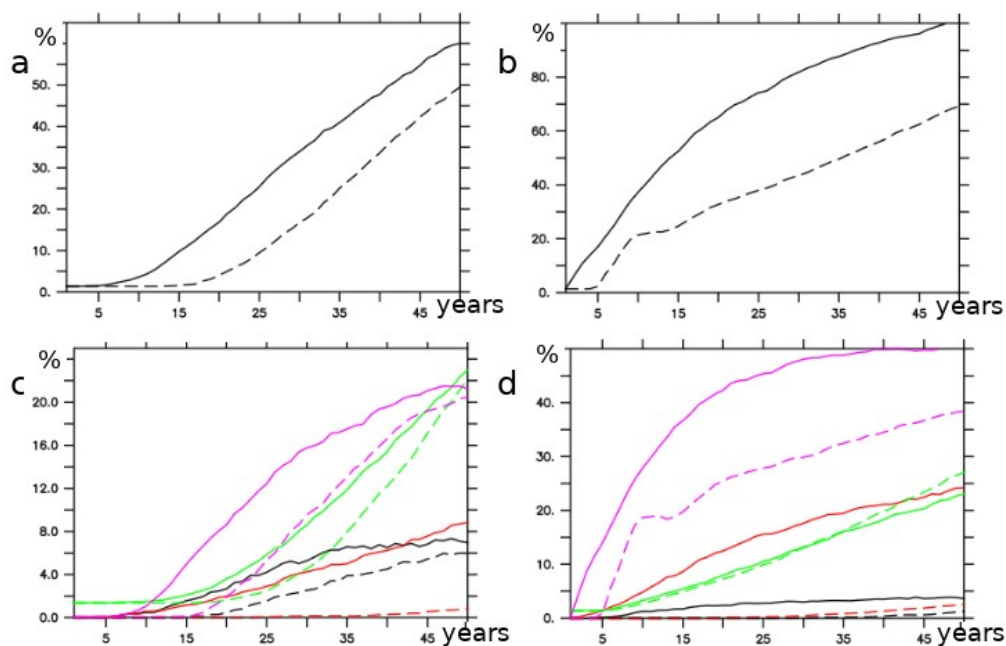
819

820 Figure 8 : a : percentage of particles originating from outside the Intermediate Eastern Tropical

821 Pacific (IETP) ocean region (release 100°W / 5°N-5°S / 1000 m) or b- originating from outside the

822 Intermediate Western Tropical Pacific (IWTP) ocean region (release 160°E / 5N°5S / 1000 m) in

823 NEMO01 (black) and NEMO05 (dash). c,d ; percentage of particles originating from outside the

824 IETP (c) and the IWTP (d): upper ocean (< 200 m) (black), deep ocean (> 2000 m) (red),

825 subtropical region (> 10°N/S) (green), panel c: western (west of 160°W) - or panel d: eastern (east

826 of 160°W) part of the basin (magenta).

827

828

829

830

831

832

833

834

835

836
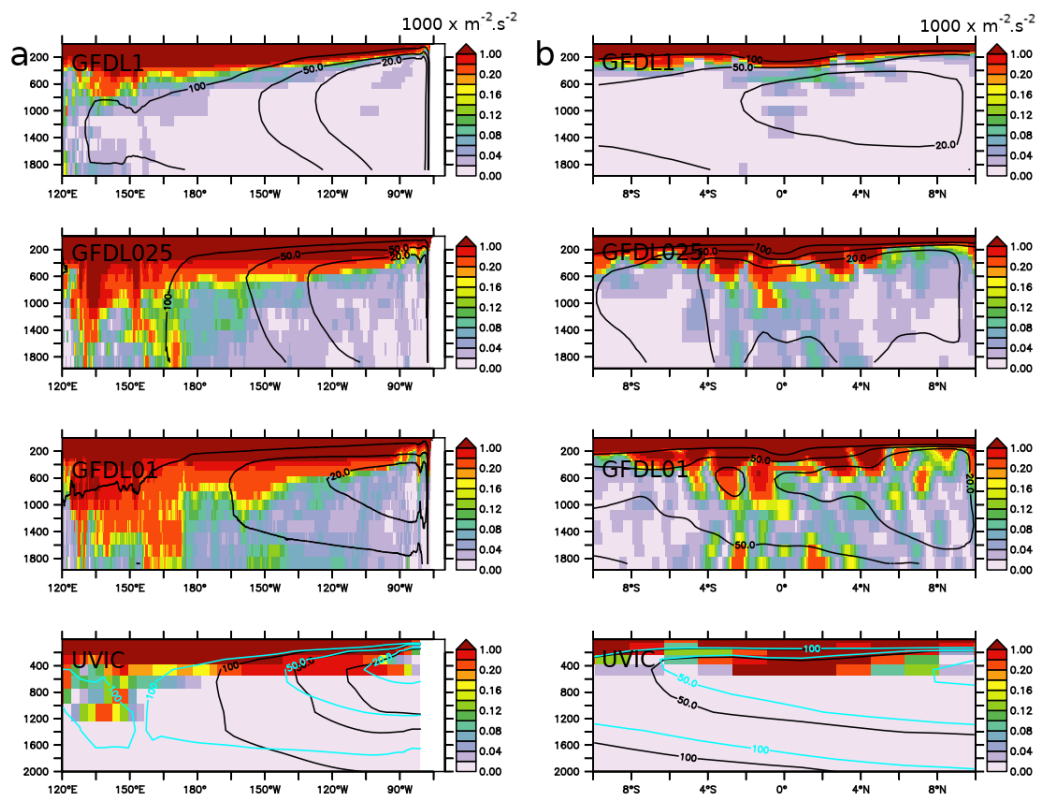
Figure 9 : a - Mean Kinetic Energy (m2.s^{-2} x 1000) (average 10°N-10°S) in GFDL01, GFDL025,

GFDL01, UVIC, b - similar to a. but average 160°W-coast. Oxygen levels (mmol.m^{-3}) are displayed

in contour. The blue contour corresponds to UVIC GD13 (Getzlaff and Dietze, 2013, including an

anisotropical increase of lateral diffusion at the equator)